Critical spin response and outer galaxy speeds

Can ESFD produce flat rotation curves?

There is a conditional route. Christopher Grenke's saturation energy supplies a spin stiffness that a universal gravitational coupling can reduce. Its vanishing defines a calculable phase boundary. If neutral, effectively zero-temperature Dirac modes also live on spin-domain interfaces, their energy produces the force exponent needed for flat outer speeds. No rotation speed, halo density profile or Tully–Fisher relation enters that derivation.

> At the phase boundary, the predicted low-acceleration force is $g - g_b \approx \sqrt{(a_D g_b)}$. Outside a finite isolated mass M this gives $v_\infty^4 = GMa_D$.

Here g_b is the inward acceleration from the ordinary stars and gas. The spin–gravity coupling, the existence of two-dimensional modes and the mechanism that keeps the stiffness at its critical value remain open. The original three-dimensional quartic spin energy alone gives a different exponent.

Test	Result
131 SPARC rotation curves	Letting the stiffness and interface strength vary selected a positive residual stiffness and zero interface term. Fixing the system at criticality changed held-out speed error only from 21.54 to 21.66 km/s.
245 external PROBES curves	Frozen predictions gave 39.19 km/s for the free fit and 39.43 km/s for the critical interface fit. Disk velocities alone gave little leverage to distinguish these limits.
Weak lensing at 300–1,000 kpc	The same two calibrations gave 106.6 and 28.6 km/s RMS error. The free disk fit declined too rapidly. Simple MOND gave 24.6 km/s on the same 16 cells.

With the reference stellar masses, two models that differ by a quarter of a km/s in external disk error differ by almost 78 km/s on the distant stacks. A 20% upward shift in the SPARC stellar masses reverses their lensing ranking. The interface hypothesis was developed after examining the quartic and spin-wave results on this previously studied archive. Its subsequent fits excluded the scored galaxies. This is a retrospective comparison.

ESFD · 4.1.docx §§3.1–3.3 and 11.2, 21.docx §3.2, November master §9 and the preceding spin-gravity study. Data · SPARC, PROBES and Mistele et al. weak lensing.

Where the critical response comes from

In 4.1.docx the saturation energy is $\lambda_s(X-\Phi_0^2)^2/4$ with $X = S_{\mu\nu}S^{\mu\nu}$. Project a rest-frame spatial spin tensor onto a dimensionless vector p, so $X = 2S_*^2|p|^2$. The quadratic coefficient becomes $a = a_{mat}-2\lambda_s S_*^2\Phi_0^2$. The saturation term contributes $4\lambda_s S_*^4$ to the quartic coefficient b_4. The clock proposal motivates a weak gravitational potential Ψ under the additional universal-lapse assumption of the preceding study.

Write $g = \nabla\Psi$ as an outward potential gradient. Matter accelerates along $-g$. A static reciprocal energy density for spin and gravity is

$$\rho_b\Psi + |g|^2/(8\pi G) - \lambda\, p\cdot g + a|p|^2/2 + b_4|p|^4/4 + D|\nabla p|^2/2.$$

Varying Ψ gives $\nabla\cdot(g-\kappa p) = 4\pi G\rho_b$, with $\kappa = 4\pi G\lambda$. The same λ drives p when the energy is varied with respect to spin. In a uniform longitudinal response or a spherical radial field, write $y = \kappa p$ and $g = g_b + y$ in signed radial components. Substitution into the spin equation gives $h_b = (a-a_c)p + b_4p^3$, where $h_b = \lambda g_b$. Consequently

$$a_c = 4\pi G\lambda^2,\ \delta = (a-a_c)/a_c,\ \chi_{long}(k) = 1/(a-a_c+Dk^2).$$

The $k = 0$ longitudinal susceptibility diverges at $a = a_c$. The transverse susceptibility of the disordered state is $1/(a+Dk^2)$. Thus gravity's feedback supplies the shift in stiffness and determines the threshold once λ is known. No evolution equation in these manuscripts selects $a = a_c$ for every galaxy.

An explicit microscopic control parameter

As a model of the manuscript's spin entropy, take n classical orientable moments per volume. Their one-site partition function is proportional to $\sinh z/z$. Its mean polarization is $\coth z - 1/z$, hence $z = 3p + 9p^3/5 + \ldots$. Entropic stiffness then contributes $a_{mat} = 3nk_BT$ and b_4 gains $9nk_BT/5$. With no other quadratic term, $T_c = [2\lambda_s S_*^2\Phi_0^2 + 4\pi G\lambda^2]/(3nk_B)$. It is a model transition temperature. The data contain no measurement of this spin temperature, density or coupling.

Saturation potential and proposed spin entropy · 4.1.docx §§3.2 and 11.2. The reciprocal energy, susceptibility and orientable-moment matching are developed here. Mean-field comparison · Arrott (1957).

Can the quartic energy alone make a plateau?

On its stable disordered branch, $g_b = \delta y + y^3/a_q^2$ with $a_q^2 = \lambda\kappa^3/b_4$. The coefficient δ measures the distance above the critical stiffness. At $\delta = 0$ the excess force is proportional to $g_b^{1/3}$ and the speed around an isolated mass eventually rises as $R^{1/6}$. For positive δ the linear term takes over in the weakest fields. At large R, g tends to $(1+1/\delta)GM/R^2$ and the speed declines as $R^{-1/2}$.

Between these limits the equations can produce a shallow stretch without imposing a flat velocity. For a compact point mass, define $t = (y/a_q)^2$. Differentiating the **total** circular speed, including baryons, gives

$$\beta = d \ln v / d \ln R = -\tfrac{1}{2} + 2t / [(\delta+3t)(1+\delta+t)].$$

Its maximum occurs at $t = \sqrt{[\delta(1+\delta)/3]}$ and equals $-\tfrac{1}{2} + 2/[3+4\delta+2\sqrt{(3\delta(1+\delta))}]$. A locally horizontal tangent is possible for positive $\delta \le 5/2-\sqrt{6} \approx 0.05051$. This condition was derived from the force law. It was never imposed on the calibration.

What the galaxies selected

Fitting all SPARC curves gave $\delta = 0.11696$ and $a_q = 5.84 \times 10^{-11}$ m/s². The five training-fold estimates of δ spanned 0.1042–0.1483. With the all-SPARC fit the shallowest possible isolated point-mass slope is −0.0763. For 10^{11} solar masses this occurs near 40.1 kpc at 209 km/s. Any complete radial doubling around that compact mass loses at least 5.15% in speed. A disk with continuing enclosed baryons can have a shallower slope or a rising curve over the same radii.

Permitting this residual stiffness reduced external rotation error from 40.64 to 39.19 km/s against the exactly critical quartic. It improved the individual error in 187 of 245 galaxies. Whole-galaxy resampling gave a conditional 95% interval of −1.64 to −1.25 km/s for the change in cohort RMS. Setting δ to zero also eliminates the eventual Keplerian decline, but the resulting unbounded slow rise misses the much larger lensing radii in the opposite direction.

Sensitivity to the assumed stellar masses

We also changed the SPARC stellar contribution by ±20% at fixed gas, recalibrated on SPARC, and left the external inputs fixed. With 20% lighter stars the free three-term model on page 4 retained a nonzero interface term and selected $\delta = 0.0850$. The critical and free models gave 24.7 and 97.0 km/s in the far lensing stacks. With 20% heavier stars both fits dropped the interface term. The free fit selected $\delta = 0.00474$ and gave 46.8 km/s versus 81.9 km/s for the critical quartic limit. The reference-mass preference is sensitive to the baryonic decomposition.

Force derivatives and fit · calibrations.csv, detuning_profile.csv, point_mass_plateaus.csv and external_paired.csv. The temperature and microscopic stiffness cannot be recovered individually from these rotation fits.

A flat-speed exponent from a Dirac spectrum

The recovered action contains a three-dimensional Dirac matter field and a Pauli spin–field term. Consider an added microscopic condition. A sign-changing gapped bulk could support an effectively two-dimensional, neutral Dirac mode on an interface. Assume its energy near neutrality is $E_{\pm}(k) = \pm\sqrt{[(\hbar v_D k)^2+\Delta^2]}$, with $\Delta = J\,p\cdot n$ for surface normal n. Such a mass response has a concrete condensed-matter realization. The archived ESFD action specifies neither these interfaces nor this coupling in galaxies. Qi, Hughes & Zhang (2008)

At zero temperature, fill the negative-energy branch of N cones. With an energy cutoff Λ, its change in energy per area is

$$-N\,[(\Lambda^2+\Delta^2)^{3/2} - \Lambda^3 - |\Delta|^3] \,/\, [6\pi(\hbar v_D)^2].$$

Expansion at small gap shifts the quadratic stiffness and leaves $\mathbf{+N|\Delta|^3/[6\pi(v_D)^2]}$. The power comes from the two-dimensional momentum measure k dk and linear dispersion. It was not set by a galaxy slope. For isotropic interface normals, the mean of $|\cos\theta|^3$ is ¼. With area per unit volume Σ, the bulk energy therefore gains $c_3|p|^3/3$ with $c_3 = \Sigma N|J|^3/[8\pi(\hbar v_D)^2]$. Use a_R for the quadratic stiffness after its cutoff-dependent shift, and retain a positive renormalized b_4.

In this cutoff model $a_R = a_{bare} - \Sigma N\Lambda J^2/[6\pi(\hbar v_D)^2]$, using $\langle\cos^2\theta\rangle = ⅓$. If a_{bare} exceeds a_c, increasing the interface area can itself drive the response through criticality. The required area density is $\Sigma_c = 6\pi(\hbar v_D)^2(a_{bare}-a_c)/(N\Lambda J^2)$. This threshold depends on short-distance matching. The model gives no mechanism that stabilizes the area at Σ_c.

$$g_b = \delta y + y^2/a_D + y^3/a_q{}^2,\ \delta = (a_R-a_c)/a_c,\ a_D = \lambda\kappa^2/c_3\ (y \ge 0).$$

At criticality the quadratic force term dominates at small y. For $g_b = GM/R^2$ it gives $y \approx \sqrt{(a_D GM)}/R$ and $v_\infty{}^4 = GMa_D$. A positive residual δ eventually restores a Keplerian decline. A proportionality scale was fitted, while the exponent and its sign followed from the state counting.

Range of the argument. Temperature, nonzero chemical potential or finite interface size rounds the cusp below its energy scale. A strict infinite-radius limit requires cold, gapless interfaces and critical tuning. A finite-T transition can give a finite scaling interval. Interacting fluctuations could change this free-fermion, mean-field result. The archived three-dimensional bulk spectrum alone supplies no two-dimensional density of states.

Original matter and saturation terms · 4.1.docx §3.2. The interface ensemble, its area density, gap matching and baryonic coupling are additional hypotheses. The release verifies the sign and coefficient by independent momentum quadrature.

A check using ordinary spin waves

There is a second mechanism that appears to give the same exponent. In a three-dimensional continuously ordered spin medium, a weak aligned source stiffens two orientational modes. Subtracting the zero-field fluctuation integral gives $\int[1/k^2-1/(k^2+m^2)]d^3k/(2\pi)^3 = m/(4\pi)$. Since m^2 is proportional to the source, the polarization change is proportional to its square root. This ordered-phase effect is well established in short-range spin models. Campostrini et al. · Engels & Mendes

Gravity changes this calculation. Only the longitudinal Fourier component of p can be followed by $g = \nabla\Psi$. Eliminating g leaves a positive penalty $a_c|P_T p|^2/2$ for nonzero wavevectors, where P_T projects perpendicular to the wavevector. In a single ordered patch take $p_0^2 = (a_c-a)/b_4$ and spin stiffness $\rho_s = Dp_0^2$. In the limit of a stiff amplitude, the two tangent modes acquire squared gaps proportional to 1 and $\cos^2\theta$, with θ the angle between order and wavevector.

Define $d = \kappa p_0$, $m_d^2 = a_c p_0^2/\rho_s$, $\varepsilon = k_B T m_d/(8\pi\rho_s)$ and $x = g_b/d$. The driven change about the ordered reference gives

$$y = \varepsilon d\, H(x),\quad H(x) = 3[\sqrt{(1+x)}-1]/2 + (x/2)\,\mathrm{asinh}(1/\sqrt{x}).$$

The angular integral uses $\sqrt{(1+x)}-1$ for one mode and averages $\sqrt{(\cos^2\theta+x)}-|\cos\theta|$ for the other. For $x \ll 1$, $H(x) = x[¾ + (\ln 2)/2 - (\ln x)/4] + O(x^2)$. Thus the weak-field correction grows relative to baryons only logarithmically. $H \approx 2\sqrt{x}$ at large x, but a dominant extra force then requires $\Delta p/p_0 = y/d > g_b/d \geq 1$. That violates the small-fluctuation expansion which produced this result.

The unrestricted SPARC fit reached exactly the square-root boundary with singular fluctuation amplitude. Restricting ε and $\Delta p/p_0$ to at most 0.1 on training radii gave 46.35 km/s external error, versus 38.07 km/s for the formal square-root shape. No scored radius combined a dominant extra force, the high-x regime and a controlled perturbation. This calculation also assumes any ordered background has been subtracted in a local frame. An isotropic galactic arrangement with a canceled background requires its own model.

Ordered-phase fluctuation integral and ESFD gravity projector · derivation here. The numerical check verifies the angular integral independently. Result tables · wave_validity.csv and cohort_scores.csv.

What the rotation curves can distinguish

All fits used actual measured galaxy speeds and the archived baryonic curves. We trained on four whole-galaxy SPARC folds and scored the fifth, then fitted on all SPARC galaxies and froze each model for PROBES. We minimized squared differences between predicted and measured speeds, weighting galaxies equally. Every model used the same observations. No outer slope or lensing point entered the fit.

Gravity law	SPARC · 131 galaxies	PROBES · 245 galaxies
Baryons alone	55.30	74.08
Exact critical quartic	21.76	40.64
Free stiffness, quartic	21.54	39.19
Critical interfaces + quartic	21.66	39.43
Free stiffness, interfaces + quartic	21.54	39.19
Pure square-root excess	22.63	38.07
Simple MOND	21.30	39.31
Previous ESFD cored law	21.52	39.56

Entries are the square root of the mean of per-galaxy mean squared speed errors, in km/s. The free combined fit set the coefficient of y^2 to zero on all five training folds and in the full SPARC fit. When δ was fixed to zero, the full sample instead gave $a_D = 1.52 \times 10^{-10}$ and $a_q = 6.69 \times 10^{-11}$ m/s^2. The slope-generating coefficient is identifiable conditional on criticality. The disk fits supply no independent evidence for surface fermions.

Outer slopes and NGC 2403

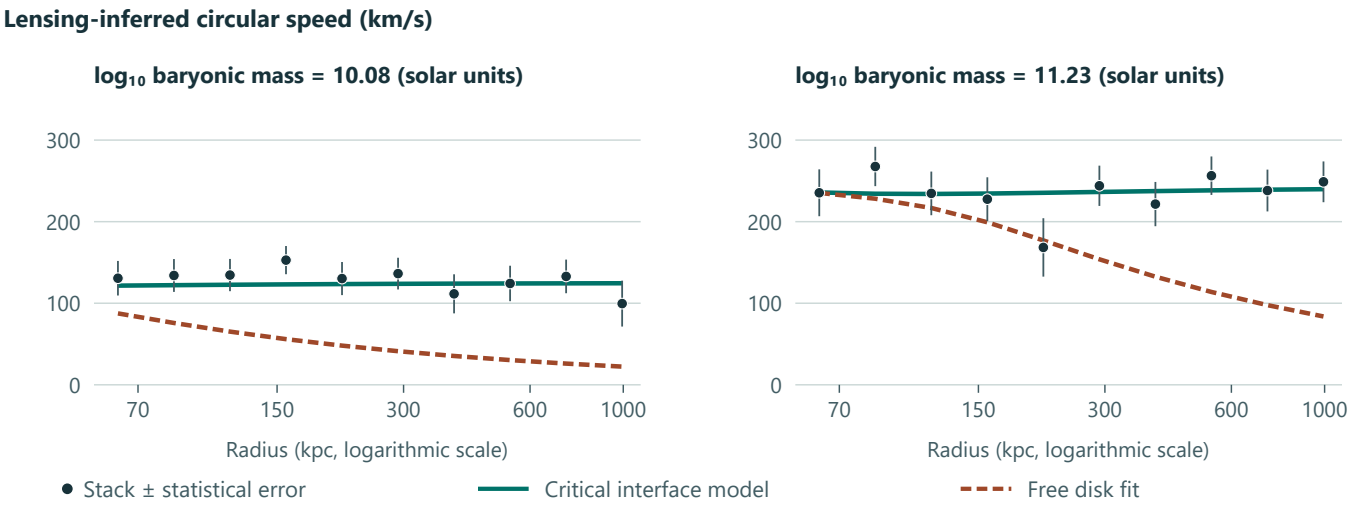
We measured d ln v/d ln R over the outer radial half in 122 SPARC and 232 PROBES galaxies with adequate sampling. For critical interfaces the median absolute slope error was 0.097 and 0.157, versus 0.133 and 0.179 for a constant-speed prediction. On the 44 SPARC curves with near-Keplerian baryonic profiles, the median observed slope was −0.061, versus −0.075 for critical interfaces and −0.088 for free stiffness. Only eight external galaxies qualified for this compact-baryon comparison.

For NGC 2403 the critical interface model predicted 124.0 km/s at 20.87 kpc, compared with 134.0 ± 3.1 km/s observed. Its full-curve error was 7.68 km/s and its outer slope was +0.035, versus +0.070 observed. The freely fitted quartic gave 7.57 km/s and +0.010. These disk calculations use the spherical algebraic force with the measured radial baryonic field. Three-dimensional disk solutions could change the numbers.

SPARC inputs · PROBES I. Results · galaxy_scores.csv, NGC2403_curve.csv and cohort_scores.csv. The earlier cubic-energy fit is the pure square-root control here.

The larger radii separate the predictions

The late-type lensing stacks extend well past the measured disks. We froze every acceleration scale at its full-SPARC value, used the tabulated mass for each bin, and compared predicted speeds with the published shear-inferred speeds. This requires equal spatial and temporal metric potentials and an approximately isolated, compact baryonic source. Neither condition follows from the spin clock by itself.



Frozen model	50–300 kpc · 24 cells	300–1,000 kpc · 16 cells
Free stiffness, quartic	63.1 km/s	106.6 km/s
Exact critical quartic	37.8 km/s	102.4 km/s
Critical interfaces + quartic	22.3 km/s	28.6 km/s
Pure square-root excess	33.8 km/s	31.4 km/s
Simple MOND	24.1 km/s	24.6 km/s

The plotted points use the publication's statistical speed errors. Additional systematic errors are retained in the accompanying table. At 300–1,000 kpc the free quartic predictions averaged 102.9 km/s below the measurements, and the exact critical quartic averaged 96.6 km/s above them. The critical interface model averaged 14.9 km/s high. For the highest mass bin at 993.86 kpc it gave 239.8 km/s, versus 248.8 ± 25.0 statistical ± 29.7 systematic km/s.

Individual outer stacks have considerable scatter. Their four measured log slopes span −0.519 to +0.090, while the critical interface slopes span +0.004 to +0.011. The table reports unweighted RMS discrepancies in amplitude. Bin mass spread, isolation, extended gas and correlated shear errors preclude a joint significance claim from these cells.

Mistele et al. (2024), weak lensing of isolated galaxies. Archived late-type table 1 and companion masses. Derived files · lensing.csv, lensing_slopes.csv and lensing_scores.csv.

How close to criticality would a galaxy have to be?

The critical-interface fit predicts flat limiting speeds of 125, 174, 206 and 242 km/s for the four published lensing masses. A small positive δ eventually stops that scaling. At a fixed measured radius we can ask how large δ could be before the linear term becomes as large as the y^2 term. This is a requirement of the fitted model, rather than a confidence interval inferred from shear.

Baryonic mass, solar units	δ for linear = quadratic at 993.86 kpc	δ for linear = 10% of quadratic
1.20×10^{10}	0.00235	0.000316
4.57×10^{10}	0.00458	0.000612
8.91×10^{10}	0.00638	0.000850
1.70×10^{11}	0.00878	0.00117

For the lowest-mass bin the renormalized quadratic stiffness must lie within about **0.24% above its critical value** for the interface term to exceed the residual linear term there, with a_D and a_q held at their critical-fit values. A ten-to-one dominance needs about 0.032%. The calculation retains the quartic correction. The free disk fit's δ ≈ 0.117 is much larger and has a different nonlinear coefficient.

Which assumptions still need physics

The coupling $-\lambda p \cdot \nabla \Psi$ used in the reciprocal energy presumes a **polar current**. Intrinsic spin in a rest frame is an axial vector. Identifying the two directly in a parity-even isotropic medium would forbid the coupling. A parity-odd background or a derived polar spin-transport current could supply the required matching. The master's entropy-weighted current is a candidate for the latter. A universal value of λ for neutral matter remains to be shown.

The observed curves fix combinations of constants, including $\lambda\kappa^2/c_3$. They do not separately fix the interface area density, Dirac velocity, spin gap J, or the independent spin susceptibility. Locating a gap proportional to spin, measuring the low-energy density of states, and measuring the current response to a separate drive would test the proposed carrier. The resolved radio measurements in the previous study constrain ordinary magnetic-field gradients. They do not measure these interface quantities.

A flat-speed law continued indefinitely gives a logarithmically growing potential. A global model with a finite lapse therefore needs an outer boundary or different physics beyond the measured range. Maintaining the requisite stiffness throughout the observed galaxies and their surroundings remains the central unresolved step for ESFD.

Calculation · criticality_scales.csv. Reproduction · research/critical_response/README.md, analyze.py and checks.py. The research bundle includes the source manuscripts, frozen galaxy inputs, numerical outputs and editable study.

Can the interface population keep itself critical?

A sign change of a bulk Dirac mass gives a concrete construction for the surface spectrum used on page 4. Let $M(z)$ have opposite signs on the two sides of an interface, with the positive side at $z > 0$. At zero in-plane momentum the Dirac equation is $[-i\hbar v_D \alpha_z \partial_z + \beta M(z)]\psi = 0$. In the $+1$ eigenspace of $i\alpha_z\beta$ its solution is proportional to $\exp[-\int_0^z M(s)ds/(\hbar v_D)]$. It decays on both sides. A mass kink $M_0 \tanh(z/L)$ gives the normalizable profile $\cosh(z/L)^{-M_0 L/(\hbar v_D)}$. The in-plane Dirac matrices preserve this subspace and yield the linear two-dimensional dispersion.

The original manuscript uses a bulk mass m. Its isotropic vector saturation energy has a connected sphere of ordered directions. A connected set of directions does not require a wall between two discrete signs. A discrete mass-generating order, anisotropy or another independent reason for mass inversion is needed. The ordinary geometric thinness of a luminous galaxy disk does not produce the required quantum spectrum.

Testing whether the threshold is selected

Write the zero-drive free energy as the sum of an interface population energy $f_{wall}(\Sigma)$ and the spin free energy. At the onset $p \to 0$ the Σ-dependent terms multiplying p^2 and $|p|^3$ vanish. Stationarity in Σ then requires $f'_{wall}(\Sigma) = 0$. Criticality separately requires $a_R(\Sigma) = 4\pi G\lambda^2$. Neither variation makes the two conditions identical. For example, positive wall tension with $f_{wall} = \sigma\Sigma + u\Sigma^2/2$, $\sigma,u > 0$, gives $\Sigma = 0$ in the disordered equilibrium. A feedback or conservation law fixing a nonzero critical area remains to be supplied.

The same example gives a way to distinguish the mechanism experimentally. Changing the interface area at fixed Dirac velocity, gap coupling J and cutoff Λ simultaneously lowers the quadratic stiffness and increases the cubic energy. In the ideal cutoff model their slopes must satisfy

$$dc_3/d(a_{bare} - a_R) = 3|J|/(4\Lambda).$$

A measurement of the gap coupling, the band scale and the two changes in the equation of state could check this relation independently of rotation curves. The cutoff-dependent ratio is specific to the specified microscopic model. The $|\Delta|^3$ exponent is the more general spectral prediction.

ESFD bulk Dirac and saturation terms · 4.1.docx §§3.1–3.3. Example of interface mass inversion and a surface Dirac mass · Qi, Hughes & Zhang. The population-energy check and linked stiffness prediction are derived here.

Can particles hold the interfaces open?

Positive surface tension shrinks an empty interface. Suppose a conserved number density n of mobile Dirac quasiparticles occupies its upper band. Spreading the particles over more area lowers their kinetic energy. Let Σ be the area per unit volume, σ the positive net tension at zero filling, N the number of cones, and $w = \hbar v_D$. The zero-temperature, zero-polarization number and energy per area are $Nk_F^2/(4\pi)$ and $Nwk_F^3/(6\pi)$. Counting the states gives the following energy per volume.

$$F(\Sigma) = \sigma\Sigma + 4\sqrt{\pi}\, w\, |n|^{3/2} / [3\sqrt{(N\Sigma)}].$$

At fixed $n \neq 0$ the minimum has $E_F = wk_F = (12\pi\sigma w^2/N)^{1/3}$ and $\Sigma = 4\pi|n|w^2/(NE_F^2)$. This yields a finite, stable area and a specific filling energy. Changing n changes the area. The minimum meets the gravitational critical-stiffness condition only for a further relation among density, tension and the microscopic couplings. The manuscripts provide no such relation.

The price of filling the surface band

Let $\Delta = Jp\cdot\hat{n}$ be the spin-dependent gap and Λ the ungapped band cutoff. For fixed number per area, upper- and lower-band energies cancel for momenta below k_F. With $H(E) = (E^2+\Delta^2)^{3/2} - E^3$, the energy change per area is $N[H(E_F) - H(\Lambda)]/(6\pi w^2)$. At zero filling $H(0) = |\Delta|^3$. For any $E_F > 0$ both terms are analytic in Δ^2 near zero. This removes the cubic energy responsible for the strictly flat limit. A nearly flat interval can survive where the spin-induced gap is large compared with the filling energy.

Write $t = \kappa E_F/|J|$ as an acceleration, $y = \kappa|p|$, and $u = |\cos\theta|$. At fixed background area and fixed filling on each patch, the neutral coefficient y^2/a_D in the force acquires the following orientation average.

$$I(y,t) = 4\int_0^1 u^2\sqrt{(t^2+y^2u^2)}\, du,\ g_b = y\, I(y,t)/a_D + y^3/a_q^2.$$

Keeping the neutral microscopic stiffness fixed gives $I = 4t/3 + 2y^2/(5t) + \ldots$ at small y. The residual linear stiffness becomes $4t/(3a_D)$, so isolated speeds ultimately decline as $R^{-1/2}$. Compensating this stiffness by hand replaces I by $I - 4t/3$. The surviving cubic force then gives $v \propto R^{1/6}$. Both cases recover $I = y$ as $t \to 0$ at fixed y.

A smooth adjustment of area cannot restore the missing cusp. Here the area stiffness is $K = 3\sigma/(2\Sigma_0)$ at equilibrium. If the quadratic spin stiffness is $r(\Sigma)$, relaxation moves the area by $-r'(\Sigma_0)p^2/(2K)$ and shifts the quartic coefficient by $-r'(\Sigma_0)^2/(2K)$. The zero-field stiffness $r(\Sigma_0)$ survives. The compensated limit assumes a positive effective quartic. The data test holds the area and particle number per patch fixed as spin responds. The tension and the rate of particle exchange between patches remain unmeasured.

The wall tension, conserved filling and spin-dependent surface gap are added hypotheses. State counting and the force are derived here. For the underlying surface spectrum see Qi, Hughes & Zhang. Numerical integration independently checks the occupied-band cancellation and angular average.

How much filling do the galaxies allow?

We kept the neutral model's two nonlinear coefficients fixed at their existing SPARC training estimates and varied only $t = \kappa E_F/|J|$. Each SPARC prediction uses a fit that excluded the whole galaxy. All 245 PROBES curves and both lensing bands use the all-SPARC calibration. Disks receive equal weight per galaxy and lensing receives equal weight per populated mass–radius cell. The earlier results on these samples were known when the new mechanism was proposed.

Model or fixed filling	SPARC · 131 disks	PROBES · 245 disks	Lensing · 16 far cells
Neutral critical interface	21.66	39.43	28.61
Filled, t fitted on SPARC	21.65	39.51	88.62
Filled, $t = 10^{-12}$ m/s²	21.66	39.43	22.86
Compensated, same t	21.68	39.36	48.79

Entries are RMS speed errors in km/s. The far lensing band spans 300–1,000 kpc. Keeping the microscopic stiffness fixed gave $t = 7.96 \times 10^{-12}$ m/s² on all SPARC. The five training-fold estimates ranged from 6.30 to 9.33 × 10^{-12} m/s². This changes the held-out disk error by only 0.009 km/s, but raises the far lensing error by 60.0 km/s. The compensated variant selected zero filling on every training fold.

At the smaller, fixed value 10^{-12} m/s² the distant discrepancy decreased. That value was one of seven points on a sensitivity grid. The lensing cells share uncertainties. Their RMS differences give no statistical detection of finite filling. Lowering the assumed stellar masses in SPARC by 20% gave far errors of 24.66 km/s for neutral interfaces and 88.05 km/s for disk-fitted filling at fixed stiffness. Raising the stellar masses by 20% set the interface weight to zero in the neutral calibration, leaving its filling unmeasurable.

Where an observation is most sensitive

For the lowest mass stack at 993.86 kpc, the neutral model gives 124.48 km/s. A 5% drop at fixed microscopic stiffness occurs at $t = 2.40 \times 10^{-13}$ m/s². When stiffness is compensated, a 5% rise occurs at 8.57×10^{-14} m/s². The observed value is 99.54 ± 28.14 statistical ± 13.54 systematic km/s. The 5% criterion describes sensitivity of the model prediction. The observation does not measure t to that precision.

For NGC 2403 at 20.87 kpc the disk-calibrated filled model predicts 122.24 km/s, compared with 123.98 for the neutral interface and 134.0 ± 3.1 observed. The local gap scale J, velocity v_D, area density and coupling κ remain unmeasured. Determining whether conserved carriers can support ESFD interfaces in a galaxy requires an independent estimate of their filling and tension.

The mass calibration and lensing assumptions follow pages 6–8. SPARC · PROBES · Lensing. Reproduce all seven supplemental tables with research/critical_response/carrier_filling.py --check.